

AEROSOL DISTRIBUTIONS AND RADIATIVE PROPERTIES SIMULATED IN THE GOCART MODEL AND COMPARISONS WITH OBSERVATIONS

Mian Chin^{1,2*}, Paul Ginoux^{1,2}, Stefan Kinne^{2,3}, Omar Torres^{2,3}, Brent Holben², Bryan N. Duncan⁴,
Randall V. Martin⁴, Jeffifer A. Logan⁴, Akiko Higurashi⁵, Teruyuki Nakajima⁶

¹Georgia Institute of Technology, Atlanta, Georgia

²NASA Goddard Space Flight Center, Greenbelt, Maryland

³University of Maryland at Baltimore County, Baltimore, Maryland

⁴Harvard University, Massachusetts

⁵National Institute for Environmental Studies, Tsukuba, Japan

⁶Center for Climate System Research, University of Tokyo, Tokyo, Japan

1. INTRODUCTION

Aerosols affect the climate directly by absorbing or scattering radiation, and indirectly by altering cloud formation and cloud properties. The magnitudes of these effects, however, are poorly constrained, because we have a limited knowledge of the processes that control aerosol distributions as well as the physical, chemical, and optical properties. Indeed, aerosol radiative forcing is one of the largest sources of uncertainty in climate change assessment (IPCC, 2001).

Here we present global model simulations of tropospheric aerosols from the Georgia Tech/Goddard Ozone Chemistry Aerosol Radiation and Transport (GOCART) model (Chin et al., 2000, 2001; Ginoux et al., 2001). The model includes major tropospheric aerosol types of sulfate, dust, organic carbon (OC), black carbon (BC), and sea-salt aerosols. The model-calculated aerosol optical thickness (τ), single scattering albedo (ω_0), and Angstrom exponent (α) are compared with satellite retrievals from the Advanced Very High Resolution Radiometer (AVHRR) and the Total Ozone Monitoring Spectrometer (TOMS) and with the ground-based sunphotometer data from the Aerosol Robotic Network (AERONET).

2. THE GOCART MODEL

2.1. General

The GOCART model is a global scale model driven by the Goddard Earth Observing System Data Assimilation System (GEOS DAS). It has a horizontal resolution of 2° latitude by 2.5° longitude and 20 to 40 vertical layers (vertical resolution depends on the version of GEOS DAS). The model contains the following modules in aerosol simulation: emission, which includes sulfur, dust, OC, BC, and sea-salt emissions; chemistry, which includes in-air and in-cloud oxidations of sulfate precursors (SO_2 and DMS); advection, which is computed by a flux-form semi-Lagrangian method; boundary layer turbulent mixing, which uses a second-order closure scheme; moist convection, which is calculated using archived cloud mass flux fields; dry deposition, which uses a resistance-in-series algorithm as a function of surface type and meteorological

conditions; and wet deposition, which accounts for the scavenging of soluble species in convective updrafts and rainout/washout in large-scale precipitation. More detailed description and references are given in Chin et al. (2000) and Ginoux et al. (2001).

2.2. Emissions

The anthropogenic emission of sulfur is taken from the Emission Database for Global Atmospheric Research (EDGAR) for 1990. Other sulfur emissions include biomass burning and volcanic emissions of SO_2 and oceanic emissions of DMS (Chin et al., 2000, 2001), Organic and black carbon emissions include anthropogenic (Cooke et al., 1999) and biomass burning emissions (B. Duncan et al., manuscript in preparation, 2001) as well as emissions of natural volatile organic carbon (Guenther et al., 1995). It should be pointed out that the biomass burning emissions are calculated based on the estimated seasonal and interannual variations of total burned biomass inventory, which is a product based on the satellite observations of fire-count and absorbing aerosol index (B. Duncan et al., manuscript in preparation, 2001). This new biomass burning database has made the modeled seasonal and interannual variations of biomass burning tracers more realistic. Dust emission is parameterized as a function of surface topography, soil type, surface wind speed and wetness (Ginoux et al., 2001). Sea-salt emission is calculated as a function of wind speed (Monahan et al., 1986). More details have been given in Chin et al. (2000, 2001) and Ginoux et al. (2001).

2.3. Size Distributions

We consider seven size bins for dust (effective radius, $r_e = 0.1-0.18, 0.18-0.3, 0.3-0.6, 0.6-1, 1-1.8, 1.8-3, 3-6 \mu\text{m}$) and four size bins for dry sea-salt ($r_e = 0.1-0.5, 0.5-1.5, 1.5-5, 5-10 \mu\text{m}$). We assume lognormal size distributions for sulfate (dry $r_e = 0.156 \mu\text{m}$), organic carbon (dry $r_e = 0.087 \mu\text{m}$), and black carbon (dry $r_e = 0.039 \mu\text{m}$) aerosols. We also assume lognormal distributions for each dust and sea-salt bins. With the exception of dust, aerosols are considered to be hydrophilic, i.e., their size increases with the increase of ambient relative humidity. Table 1 lists the hygroscopic growth factors of effective radius at different

ambient relative humidity in our model, based on the Global Aerosol Data Base (Köpke et al., 1997).

Table 1. Hygroscopic growth factors $r_e/r_{e, \text{dry}}$ at different RH.

RH(%)	0	50	70	80	90	95	99
Sulfate	1	1.4	1.5	1.6	1.8	1.9	2.2
OC	1	1.2	1.4	1.5	1.6	1.8	2.2
BC	1	1.0	1.0	1.2	1.4	1.5	1.9
Sea-Salt	1	1.6	1.8	2.0	2.4	2.9	4.8

2.4. Radiative Properties

The radiative properties include the extinction coefficient (Q), single scattering albedo (ω_0), and asymmetry factor (g). These properties, which are size and wavelength dependent, have been calculated using the Mie theory with the refractive indices from Köpke et al. (1997) and the size distributions described above. For hydrophilic aerosols the effective refractive indices are obtained by volume weighing of the dry aerosol and water.

The aerosol optical thickness (τ) is calculated as follows. For each aerosol type or size at a given wavelength, the optical thickness τ is

$$\tau = \frac{3QM}{4\rho r_e} \quad (1)$$

where Q is the extinction coefficient, M is the aerosol mass loading, ρ is the density, and r_e is the effective radius. All these quantities are defined in an ambient RH environment.

Given the model simulated aerosol dry mass, equation (1) can be re-written as

$$\tau = \beta M_d \quad (2)$$

where β is called specific extinction or mass extinction efficiency ($\text{m}^2 \text{g}^{-1}$), which is simply the quantities in the right hand side of equation (1) divided by the dry aerosol mass M_d , i.e.,

$$\beta = \frac{3QM}{4\rho r_e M_d} \quad (3)$$

so that all the humidification effects are embodied in the value of β .

Figure 1 demonstrates the relative humidity and wavelength dependence of β for hygroscopic aerosols. Figure 1a shows that at 80% RH, the β 's at 500 nm for sulfate, OC, and sea-salt aerosols are about a factor of 2-3 greater than their dry values, whereas at 99% RH the β 's are a factor of 10 greater for sulfate and OC, and about 20 for sea-salt. For the hydrophilic BC, it starts growing only when $\text{RH} > 70\%$, and its β increases at a factor of 2.5 at 99% RH from the dry value. The β enhancement factors calculated here are consistent with those measured in the Tropospheric Aerosol Radiative Forcing Observational

Experiment (TARFOX) where a factor of 1.81 – 2.31 at wavelength of 550 nm was found as the ratio of light scattering efficiency at 80% RH to that at 30% (Kotchenruther et al., 1999). Figure 1b plots the wavelength dependence of β for hygroscopic aerosols at 4 different sizes, corresponding to RH at 0, 30, 80, and 95% (number and r_e for these sizes indicated in Figure 1a). There is a strong decrease in β with the increase of wavelengths for sulfate, OC and BC at UV and visible spectral regimes, in contrast with sea-salt aerosol, which shows little variation at those wavelengths due to its relatively large size. The more the water is taken up by the aerosol particles, the higher the extinction efficiency will become.

3. Results

3.1. Contributions of Individual Aerosol Types to the Total Aerosol Optical Thickness

The annual averaged total aerosol optical thickness at 500 nm from our standard simulations for 1990 is shown in Figure 2. Globally, the averaged AOT at 500 nm in 1990 is 0.040 for sulfate, 0.017 for organic carbon, 0.007 for black carbon, 0.051 for dust, and 0.027 for sea-salt. The contributions of each individual aerosol types to the total aerosol optical thickness are also shown in Figure 2. Sulfate aerosol is mainly concentrated in three major pollution regions: eastern North America, Europe, and eastern Asia. Carbonaceous aerosols (OC + BC) are optically the most important aerosols over the equatorial South America and Africa mainly over the biomass burning regions. Dust aerosol dominates the total τ in latitudinal band of 10°S-40°N over the Atlantic and Indian oceans as well as over the source regions of northern Africa, Asia, and Australia. In the southern hemisphere, sea-salt is the major type of aerosol at latitudes higher than 30°S where it contributes 40-80% to the total τ .

3.2. Comparison with Satellite Retrievals from TOMS and AVHRR

3.2.1 Global distribution of optical thickness

Two of the satellite sensors, AVHRR and TOMS, have been measuring aerosol signal for more than 20 years at either visible (AVHRR) or ultraviolet (TOMS) wavelengths. There are several retrieval algorithms to extract the aerosol optical thickness from the AVHRR measured backscatter radiation, using either one channel retrieval (Stowe et al., 1997) or two-channel retrieval technique (Nakajima and Higurashi, 1998; Mishchenko et al., 1999; Higurashi et al., 2000). Because of the highly variable land surface reflectance of the visible wavelengths, the AVHRR retrieval cannot derive aerosol information over the land. In contrast, the retrieval products from the TOMS measurements cover both land and ocean, since the TOMS instrument measures backscattering at the UV wavelengths which have low and nearly constant reflectance at most surfaces (Herman and Celarier, 1997). The TOMS products, therefore, provide unique information of

aerosol sources, which are all located over the land except sea-salt. Aerosol products from the TOMS retrieval include aerosol index (AI) which is the ratio of the backscatter signals from the two TOMS UV channels (Herman et al., 1997), and aerosol optical thickness at 380 nm (Torres et al., 2001).

We compare the seasonal variations of modeled total aerosol optical thickness with the TOMS data for 1997 (Figure 3) and the AVHRR data for 1990 (Figure 4). Two different versions of the AVHRR products are shown in Figure 4: one is the NOAA operational product from one-channel (630 nm) retrieval algorithm (Stowe et al., 1997, hereafter AVHRR-1), while the other is from two-channel (630 and 840 nm) retrieval algorithm (Higurashi et al., 2000, hereafter AVHRR-2). The TOMS and AVHRR-2 data were converted to commonly referred wavelengths of 550 nm (Torres et al., 2001) or 500 nm (Higurashi et al., 2000). Because cloud screening algorithms in the satellite retrieval have rejected a large amount of raw data, the satellite data shown in Figure 3 and 4 are monthly composite rather than monthly average.

Both the TOMS data and the model results (Figure 3) show that the highest values of τ are persistently located over the northern Africa where dust is the predominant aerosol component, except in the biomass burning season (e.g., January) when carbonaceous aerosols are also important there. High dust τ values over Taklimakan and Gobi deserts in Asia and over Arabia peninsular are also seen from the model, matching the locations of "hot spot" in the TOMS products. Transport of the aerosol plume from northern Africa to the Atlantic Ocean is the most visible feature from both the model and the satellite products (Figure 3 and 4). During the burning seasons (e.g., July and October in Figure 3 and 4), high τ values from biomass burning aerosols are also located at the west coast of southern Africa. Another feature from the model is the sea-salt band near 60°S for all seasons, a feature that is particularly evident from the AVHRR-1 data. The model shows an interannual variability of τ between the two different years of 1990 and 1997 (first column in Figure 3 and 4), with the most notable difference in October. While it is only 0.05 – 0.2 in 1990, the τ over Indonesia has reached values above 1 in 1997 due to the intensive biomass burning started in September. A similar τ value is also shown in the TOMS data for 1997 (Figure 3). The modeled τ over the ocean in 1997 is also higher than that in 1990, largely a result of the higher sea-salt emission in 1997.

One major discrepancy between the model and the satellite data is that the model has a much stronger latitudinal gradient over the ocean. The satellite data generally show little latitudinal contrast, but the model shows a band with minimum τ values over the southern tropical ocean between 0° and 30°S, typically a factor of 2 – 3 lower than the values at northern mid and high latitudes. Such a latitudinal gradient is a common feature among most of the global aerosol models (Penner et al., 2001). Difficulties in retrieving low τ values at remote ocean from the satellite measurements may explain the discrepancy, although in-

creasing sea-salt or biogenic sulfur emissions at southern tropical ocean in the model would reduce the gradient and bring a better match between the model results and the satellite data (Penner et al., 2001).

Figure 4 clearly reveals the discrepancy in the two AVHRR retrieval products. While the difference is small over the regions where τ values are relatively high, such as off the west coast of northern Africa, the τ over the remote oceans from AVHRR-1 is more than a factor of 2 lower than that from AVHRR-2. Although the τ 's are at 630 nm from AVHRR-1 which are expected to be slightly lower than those at 500 nm from AVHRR-2, the differences shown in Figure 4 are much too large to be explained by the τ 's at different wavelengths. Differences in retrieval techniques and assumptions of aerosol properties are likely the cause of the differences in the two AVHRR products.

3.2.2 Regional comparisons of optical thickness

To achieve a more quantitative comparison, we extract the model results and the satellite data from selected regions over the land and ocean (Figure 5). These regions are chosen to represent the source, outflow, or remote environment and with sufficient satellite coverage for all seasons. The eight land regions include three major pollution source regions (L1: United States, L2: Europe, L3: East Asia), two dust source regions (L4: northern Africa, L5: Asia), two biomass burning regions (L6: Brazil, L7: southern Africa), and Australia (L8). The eight ocean regions include those influenced by continental outflow (O1 – O4), Saharan dust outflow (O5), biomass burning outflow (O6), and those at remote oceans (O7: southern Indian Ocean, O8: southern tropical Pacific). Note that O7 can be influenced by biomass burning aerosols (Figure 2) during the burning seasons. Aerosol over the continental outflow regions is usually composed by several different types (Figure 2), and the relative importance of individual type varies with the season. The regional comparisons are presented in Figure 6 where the model results are compared with the TOMS (Figure 6a and 6b) and AVHRR (Figure 6c and 6d) data at similar wavelengths for the same time periods in Figure 3 and 4. The comparison with AVHRR is limited to oceanic regions because there were no AVHRR retrievals over the land.

Figure 6a shows that the model and the TOMS data agree to within 25% over the major pollutions source regions (L1 – L3) for all seasons, and to within 40% over the dust source regions (L4 and L5) except for January over northern Africa when the modeled τ is a factor of 2 higher than the TOMS data. Over the biomass burning regions (L6 and L7), the model agrees with the TOMS data to within 10 – 50% during the burning seasons (July and October), but in the non-burning seasons the background τ 's from the model are 4 to 5 times lower than those from the TOMS data. Over Australia (L8), the modeled τ 's are around 40% of the TOMS values except in October 1997 when, influenced by biomass burning emissions, the model and the TOMS agree.

Over the ocean, the modeled τ 's agree with both TOMS (Figure 6b) and AVHRR-2 (Figure 6d) to within 0

– 40% at regions that are affected by continental (O1 – O4) or dust outflow (O5). Over the biomass burning outflow region (O6), the discrepancy between the model and the satellite data is similar to that over the biomass burning source regions (L6 and L7): the modeled τ 's are 2 to 5 times smaller than the satellite data in the non-burning seasons, but the agreement is within 35% during the burning season. The largest discrepancy between the model and the TOMS or AVHRR-2 lies, as we have seen in Figure 3 and 4, at the remote oceanic regions in the southern hemisphere (O7 and O8), where the modeled τ 's are 0.05 to 0.15 in 1997 and 0.04 to 0.10 in 1990, which are 2 to 5 times lower than the τ 's from TOMS and AVHRR-2. This suggests that either the model has significantly underestimated aerosol source in the remote ocean, or the TOMS and AVHRR-2 retrievals have overestimated the background aerosol level due to the large uncertainties at low aerosol signals. In contrast, the lower τ from AVHRR-1 (Figure 6c) retrieval brings a better agreement with the model results over the remote regions compared to AVHRR-2, but worsens over the continental outflow regions (O1 – O4). In general, the model agrees better with AVHRR-1 than AVHRR-2 over the remote oceans, but the reverse is the case over the outflow regions.

3.2.3 Ångström exponent

Another product from the 2-channel AVHRR retrieval is the Ångström exponent (α) of aerosols (Higurashi et al., 2000), which is the measure of wavelength dependent of the aerosol optical thickness, defined as

$$\alpha = \frac{\ln(\tau_1/\tau_2)}{\ln(\lambda_1/\lambda_2)}$$

where τ_1 and τ_2 are optical thickness at wavelength λ_1 and λ_2 , respectively. Generally speaking, smaller particles (submicron size) have stronger wavelength dependence in light extinction than larger particles (Figure 1).

Figure 7 shows the α from the model (at wavelengths 600 and 800 nm) and from the AVHRR-2 retrieval (at 630 and 840 nm) for January, April, July, and October 1990. There are a number of similarities but also a number of differences between the model and the AVHRR-2 data. The regions where the model and the satellite agree relatively well include the tropical and subtropical Pacific Ocean near the coast of North and South America, tropical Pacific and Indian oceans around Indonesia where small particles (sulfate and carbonaceous) dominate, and tropical North Atlantic off the west coast of Africa where dust is the most important aerosol type. The major discrepancy lies at the tropical and southern Atlantic, areas heavily influenced by biomass burning activities. The modeled α there is usually between 1.2 and 2 during the burning season, reflecting the dominant presence of the small size carbonaceous aerosol particles, while the AVHRR-2 data show the α values generally below 1. Over the mid-latitude oceans in July, the α values from the AVHRR-2 are above 1.5, compared with the model calculated values below 1.

3.3. Comparison with sunphotometer measurements from AERONET

3.3.1 Optical thickness

The AERONET program is a federation of the ground-based sunphotometer measurement network which, started in 1993 at more than a dozen sites, has grown rapidly to over 100 sites worldwide (Holben et al., 2001). The AERONET has been providing column integrated aerosol optical properties at 8 wavelengths from 340 nm to 1020 nm. Here we compare our model results with the AERONET measurements of τ at 500 nm at 20 sites, where the data are quality assured with two or more years of measurements available (Holben et al., 2001).

The comparisons are shown in Figure 8. The period of AERONET measurements varies with sites, as indicated in Figure 8, while the model results are the average of 1996 and 1997, a period that has been included in most of the AERONET measurement sites. The first four sites in Figure 8 are predominantly influenced by biomass burning aerosols: Mongu in southern Africa, Cuiaba, Los Fieros, and Brazilia in Brazil. The model shows that the biomass burning activity peaks in September at these four sites, consistent with the AERONET measurements. The model simulated seasonal variation has improved significantly from the previous studies (see Chin et al., 2001) because of a more realistic biomass burning emission dataset used in this study (section 2.4). However, the magnitude of the maximum τ at three South American sites is underestimated in the model by a factor of 2-3, suggesting that the biomass burning emission in the model is probably too low in Brazil during the burning season.

Sites 5-8 in Figure 8 are located in northern Africa and are influenced by both dust aerosol and carbonaceous aerosol from biomass burning. The relative importance of these two types of aerosol depends on the season. In winter months the carbonaceous aerosol is important and stands as the major aerosol type at site 5 and 6, while dust aerosol dominates the remainder of the year. However, the modeled τ 's are too low in spring time at these sites, although in general they still rest within the standard deviations of the data. The strong perturbation over the local dust source, which is not resolved in the model, might explain the discrepancies (Ginoux et al., 2001).

Aerosols in sites 9-12 in Figure 8 consist mainly of mineral dust: Dalanzadgad located in the Gobi desert, Bahrain and Sede Boker in the middle east, and Cape Verde off the west coast of northern Africa. The model overestimates τ at Dalanzadgad from April to December, a problem which may be related to the possibility that too large a fraction of small dust particles ($r_e \leq 1.5 \mu\text{m}$) have emitted from the Taklimakan and Gobi dessert (Ginoux et al., 2001). Consequently, the amount of dust being transported out from Asia may be overestimated because smaller dust particles have longer lifetime and are subject to more efficient long-range transport than larger particles (Ginoux et al., 2001). The model reproduces closely the observed seasonal variation at Bahrain, Sede Boker, and

Cape Verde, although the modeled τ values are 20 – 40% higher than the AERONET data at the former two sites.

Sites 13-16 are generally considered as being dominated by pollution aerosols: Ispra in Italy, Goddard Space Flight Center at suburban Washington D.C., Bondville in Illinois, and the CART site in Oklahoma. The model results do show that sulfate aerosol from anthropogenic sources is a major component at these sites, followed by dust aerosol. Despite the fact that the calculated τ values are within the uncertainty range of the observations, high α (1.0 - 1.8) from the AERONET retrieval indicates that aerosols at these sites are mainly composed by small particles (Holben et al., 2001) rather than dust. This suggests that the background level of dust aerosol in the model is probably too high.

The last 4 sites in Figure 8 contain various aerosol types. The model results show that at Bermuda and Dry Tortugas dust is the major aerosol type, mainly from the long range transport from Africa, while in winter and early spring other aerosol types are equally important. The model misses the spring maximum as shown in the AERONET data at these two sites. The seasonal variation of τ at Seville is simulated by the model, with dust as a primary source in the spring and sulfate in the summer, though the τ is a factor of 2 too high in the model. Finally, at the oceanic site of Lanai (Hawaii), the modeled τ values are too high, especially from May to October, a bias that can be partly attributed to the possible overestimate of small dust particle emissions from Asia, as seen at Dalanzadgad (site 9). The small particles can be efficiently uplifted to 7-8 km altitude and subsequently transported to large areas over the North Pacific Ocean (Ginoux et al., 2001).

3.3.2 Ångström exponent and single scattering albedo

The α values from the AERONET measurement were obtained by linear fitting of aerosol optical thickness at 4 wavelengths between 440 and 870 nm (Holben et al., 2001). Figure 9 compares the model calculated α for wavelength 450 and 900 nm at the same 20 AERONET stations as in Figure 8. At the biomass burning aerosol dominated sites (1-4), the model reproduces quite well the AERONET derived α in both seasonal variations and values. Model also agrees with AERONET data at the dust dominated site of Cape Verde. At other sites the agreement is less satisfactory, although the seasonal variations are reproduced by the model in most of the sites. Considering the level of agreement in the aerosol optical thickness shown in Figure 8, the discrepancy in α here suggests that the partition of aerosol types in the model may not be accurate, for example, there are too much large particles such as dust at Ispra or GSFC, or not enough small particles there such as sulfate.

The model calculated column effective aerosol single scattering albedo, ω_0 , at 500 nm are also compared with the AERONET retrievals (Dubovik et al., 2001) in Figure 10. The modeled ω_0 values are almost always lower than those from the AERONET retrieval, indicating that the imaginary part of the refractive indices for absorbing aero-

sols may be too high. For example, the refractive index of dust used in the model at wavelength of 500 nm is 1.53-0.0078i (Köpke et al., 1997; Patterson, 1977). It is suggested from the observations that the value of the imaginary part is too high (Kaufman et al., 2001).

4. Concluding Remarks

We have use the GOCART model to simulate the aerosol optical thickness for major types of tropospheric aerosols including sulfate, dust, OC, BC, and sea-salt. The GOCART model uses a dust emission algorithm that quantifies the dust source as a function of the degree of topographic depression, and a biomass burning emission source that includes seasonal and interannual variability based on the satellite observations. These physically and observationally based aerosol emissions, along with the use of assimilated meteorological fields, have made the model suitable for comparisons with observations conducted at a wide range of spatial and temporal scales.

Model-calculated τ 's have been compared with the most recent satellite products from the TOMS retrieval over both land and ocean and with both one- and two-channel retrieval products from the AVHRR over the ocean. The model reproduces the prominent features of geographical and temporal variations of τ 's as observed by the satellites, such as dust plumes over northern Africa and Arabia Peninsular, biomass burning plumes in southern Africa, the intense biomass burning signal over Indonesia in October 1997, sea-salt band at high latitudes, and the seasonal shift of the latitudinal locations of the aerosol plume off the west coast of northern Africa. While there are clear differences among the satellite products, a major discrepancy between the model and the satellite data is that the model shows a much stronger variation of τ from source to remote regions. The model results and the satellite data agree to within a factor of 2 over the aerosol source and outflow regions, but they are typically a factor of 2 to 5 lower than the TOMS and the two-channel AVHRR retrieval data over the remote regions or under background conditions. Cloud contamination and the low sensitivity at low aerosol levels in the satellite retrieval are likely the main reasons to cause the discrepancy, although we cannot exclude the possibility that the sources, such as sea-salt emission, are severely underestimated in the model in the remote regions.

The comparisons of model results with the data from the AERONET sites have shown that the model reproduces the seasonal variations at most of the sites, especially the places where biomass burning or dust aerosol dominates, even though the magnitudes do not always match the observations. At areas near or influenced by Asian dust source, the modeled τ is too high, which may be attributed to an overestimate of the fraction of small dust particle emissions from the Asian desert followed by efficient long-range transport to large areas over the North Pacific.

We have also compared the model calculated Ångström exponent, α , over the oceans with the AVHRR re-

retrieval and the AERONET data. The model agrees with the AVHRR retrieval at the west coast of North and South America, Tropical Pacific, and the west coast of northern Africa, but the model calculated α values are much higher than the AVHRR in southern Atlantic region which is influenced heavily by the biomass burning aerosols. The model reproduces the α determined from the AERONET at the sites predominated by biomass burning and dust aerosol, but underestimates the α values at most of the other sites. When comparing the column effective single scattering albedo ω_0 with the AERONET retrieval, the modeled values are almost always lower than that from the AERONET, suggesting that a lower imaginary part of the refractive index for absorbing aerosols than that used in the model is probably more realistic.

Still, there are difficulties and problems in the quantitative comparison of model results with the satellite data, caused by large uncertainties involved in deriving the τ 's by both the model and satellite retrieval. For models, the uncertainties include processes associated with the simulation of aerosol mass (emission, chemistry, transport, and removal) and parameters used in calculating the mass extinction efficiency (hygroscopic properties, refractive indices, and mixing state). For satellite retrievals, the uncertainties involve the cloud screen method, surface reflectance, and assumptions in aerosol properties. Furthermore, there are inconsistencies between the model and satellite retrieval in terms of the exclusion of clouds, assumption of aerosol types, and microphysical and optical parameters in deriving the τ values. At present, the comparison of the model and satellite results can be meaningfully interpreted only in regions where the τ 's are high and dominated by one type of aerosols, such as near African dust source area or intensive biomass burning regions. More effort should be made to study the sensitivity of the τ to the uncertainties in the model and in the satellite retrieval. Finally, more comprehensive comparisons with the AERONET measurements of aerosol properties and closely coordinated investigations between modeling, field experiments, and satellite retrieval should be pursued to reduce these uncertainties.

References

- Chin, M., R. B. Rood, S.-J. Lin, J.-F. Muller, and A. M. Thompson, 2000a: Atmospheric sulfur cycle simulated in the global model GOCART: Model description and global properties, *J. Geophys. Res.*, 105, 24,671-24,687.
- Chin, M., P. Ginoux, B. Holben, M.-D. Chou, S. Kinne, and C. Weaver, 2001: The GOCART model study of aerosol composition and radiative forcing, in the *Special Volume for A Millennium Symposium on Atmospheric Chemistry*, 81st AMS Annual Meeting, American Meteorological Society.
- Cooke, W. F., C. Lioussé, H. Cachier, and J. Feichter, 1999: Construction of a $1^\circ \times 1^\circ$ fossil fuel emission data set for carbonaceous aerosol and implementation and radiative impact in the ECHAM4 model, *J. Geophys. Res.*, 104, 22,137-22,162.
- Dubovik, O., B. N. Holben, T. F. Eck, A. Smirnov, Y. J. Kaufman, M. D. King, D. Tanré, and I. Slutsker, 2001: Variability of absorption and optical properties of key aerosol types observed in worldwide locations, *J. Atmos. Sci.*, in press.
- Ginoux, P., M. Chin, I. Tegen, J. Prospero, B. Holben, O. Dubovik, and S.-J. Lin, 2001: Sources and distributions of dust aerosols simulated with the GOCART model, *J. Geophys. Res.*, in press.
- Guenther, A. et al., 1995: A global model of natural volatile organic compound emissions, *J. Geophys. Res.*, 100, 8873-8892.
- Higurashi, A., T. Nakajima, B. N. Holben, A. Smirnov, R. Frouin, and B. Chatenet, 2000: A study of global aerosol optical climatology with two-channel AVHRR remote sensing, *J. Climate*, 13, 2011-2027.
- Holben, B. N., et al., 2001: An emerging ground-based aerosol climatology: Aerosol optical depth from AERONET, *J. Geophys. Res.*, 106, 12,067-12,098.
- Intergovernmental Panel on Climate Change, 2001: *Climate Change 1994: Radiative Forcing of Climate Change*, edited by J. T. Houghton et al., Cambridge University Press.
- Kaufman, Y. J., D. Tanre, O. Dubovik, A. Karnieli, and L.A. Remer, 2001: Absorption of sunlight by dust as inferred from satellite and ground-based remote sensing, *Geophys. Res. Lett.*, 28, 1420-1482.
- Köpke, P., M. Hess, I. Schult, and E. P. Shettle, 1997: Global aerosol data set, *Rep. no. 243*, Max-Planck Institut für meteorologie, Hamburg.
- Mishchenko, M. I., I. V. Geogdzhayev, B. Cairns, W. B. Rossow, and A. A. Lacis, 1999: Aerosol retrievals over the ocean by use of channels 1 and 2 AVHRR data: Sensitivity analysis and preliminary results, *Appl. Optics*, 38, 7325-7341.
- Monahan, E. C., D. E. Spiel, and K. L., Davidson, 1986: A model of marine aerosol generation via whitecaps and wave disruption, in *Oceanic Whitecaps*, edited by E. C. Monahan and G. Mac Niocaill, pp. 167-174, D. Reidel, Norwell, Mass.
- Nakajima, T., and A. Higurashi, 1998: A use of two-channel radiances for an aerosol characterization from space, *Geophys. Res. Lett.*, 25, 3815-3818.
- Olivier, J. G. J., A. F. Bouwman, C. W. M. Van der Maas, J. J. M. Berdowski, C. Veldt, J. P. J. Bloss, A. J. H. Vesschedijk, P. Y. J. Zandveld, and J. L. Haverlag, 1996: A set of global emission inventories of greenhouse gases and ozone-depleting substances for all anthropogenic and most natural sources on a per country basis and on $1^\circ \times 1^\circ$ grid, *RIVM/TNO Rep. 771060 002*, Rijkinstituut voor Volksgezondheid en Milieu, Bilthoven, Netherlands.
- Stowe, L. L., A. M. Ignatov, and R. R. Singh, 1997: Development, validation, and potential enhancements to the second-generation operational aerosol product at the National Environmental Satellite, Data, and Information Service of the National Oceanic and Atmospheric Administration, *J. Geophys. Res.*, 102, 16,923-16,934.
- Torres, O., P. K. Bhartia, J. R. Herman, A. Sinyuk, P. Ginoux, and B. Holben, 2001: A long-term record of aerosol optical depth from TOMS observations and comparison to AERONET measurements, *J. Atmos. Sci.*, in press.

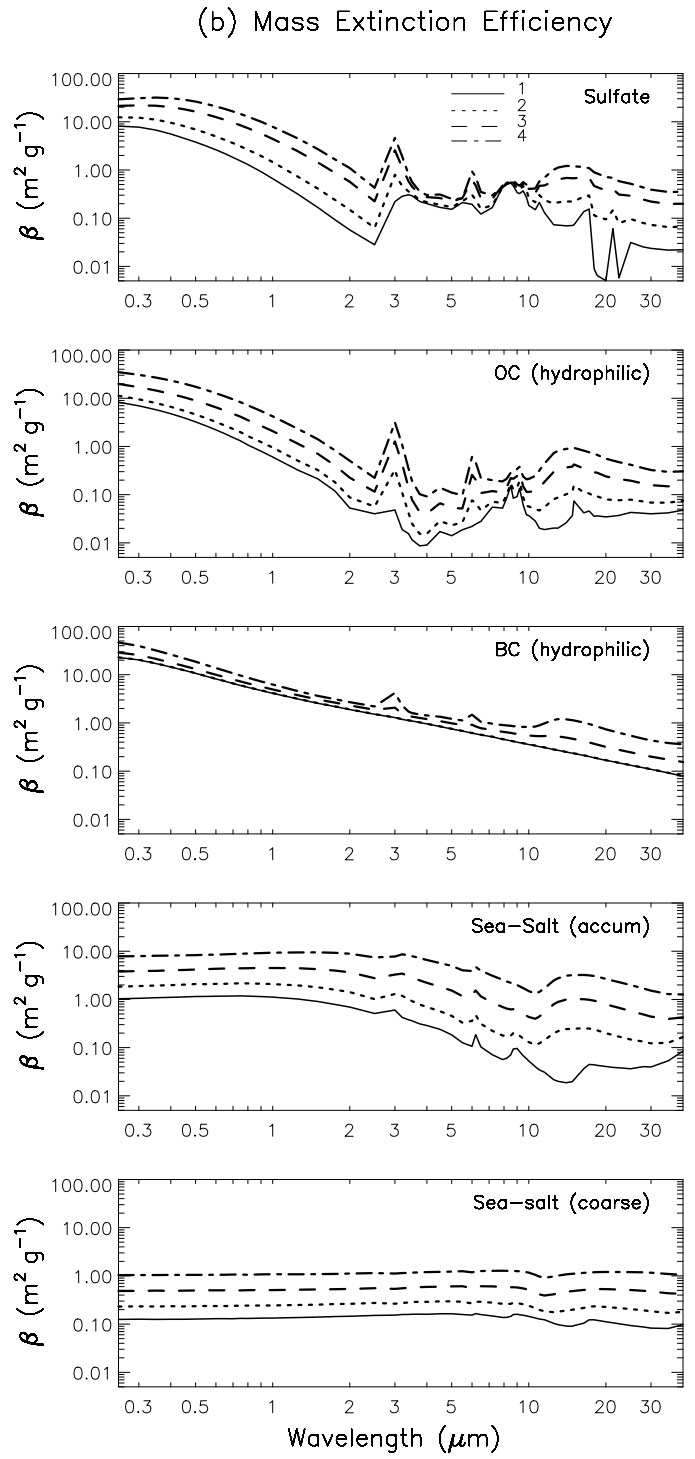
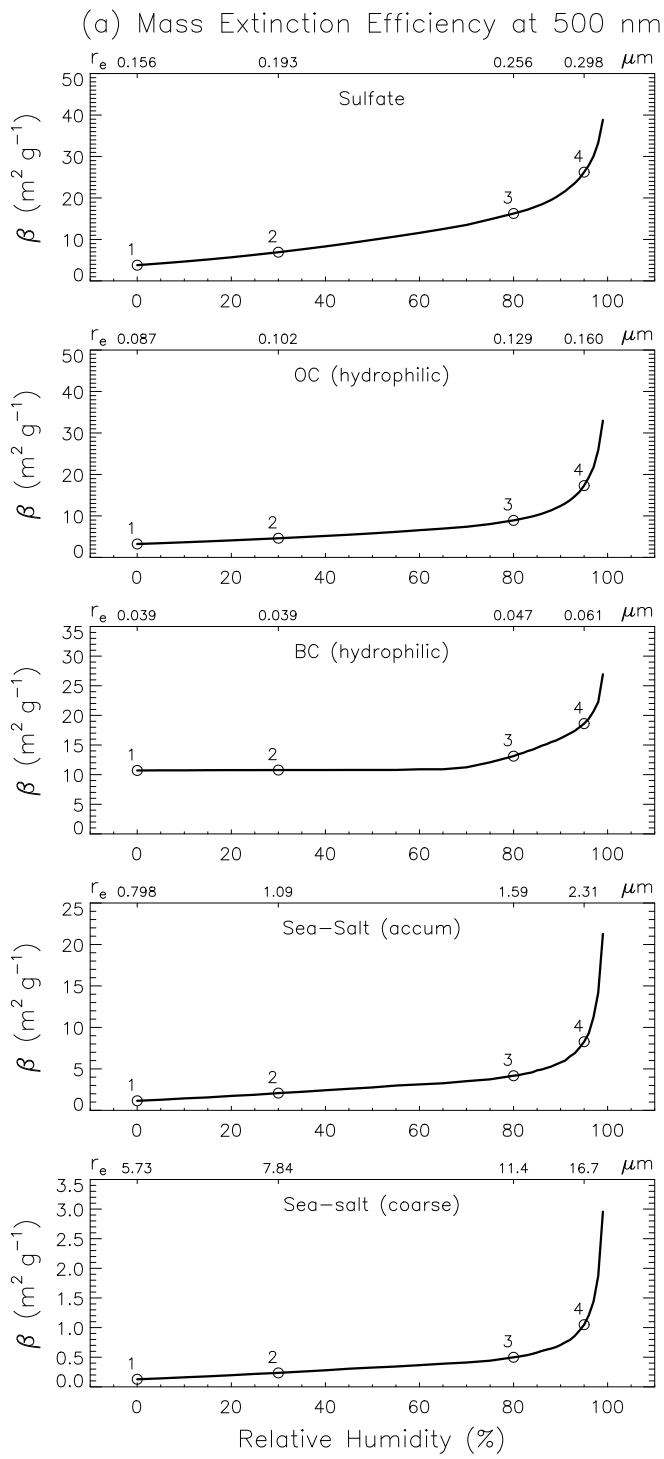


Figure 1

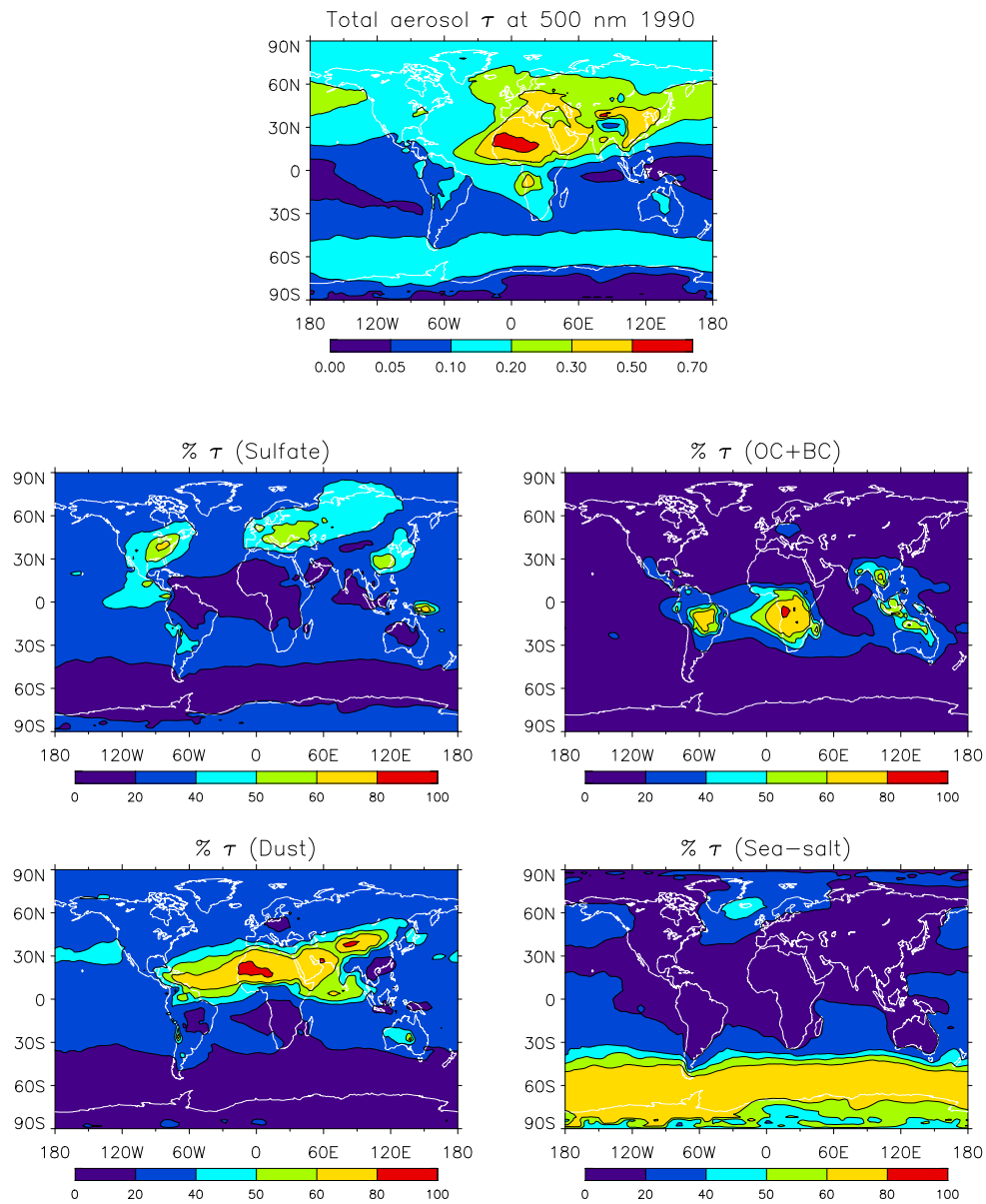


Figure 2. GOCART model calculated annually averaged total aerosol optical thickness at 500 nm (top panel) and the contributions (%) of individual aerosol component to the total optical thickness. Results are for 1990, under all sky conditions (clear and cloudy).

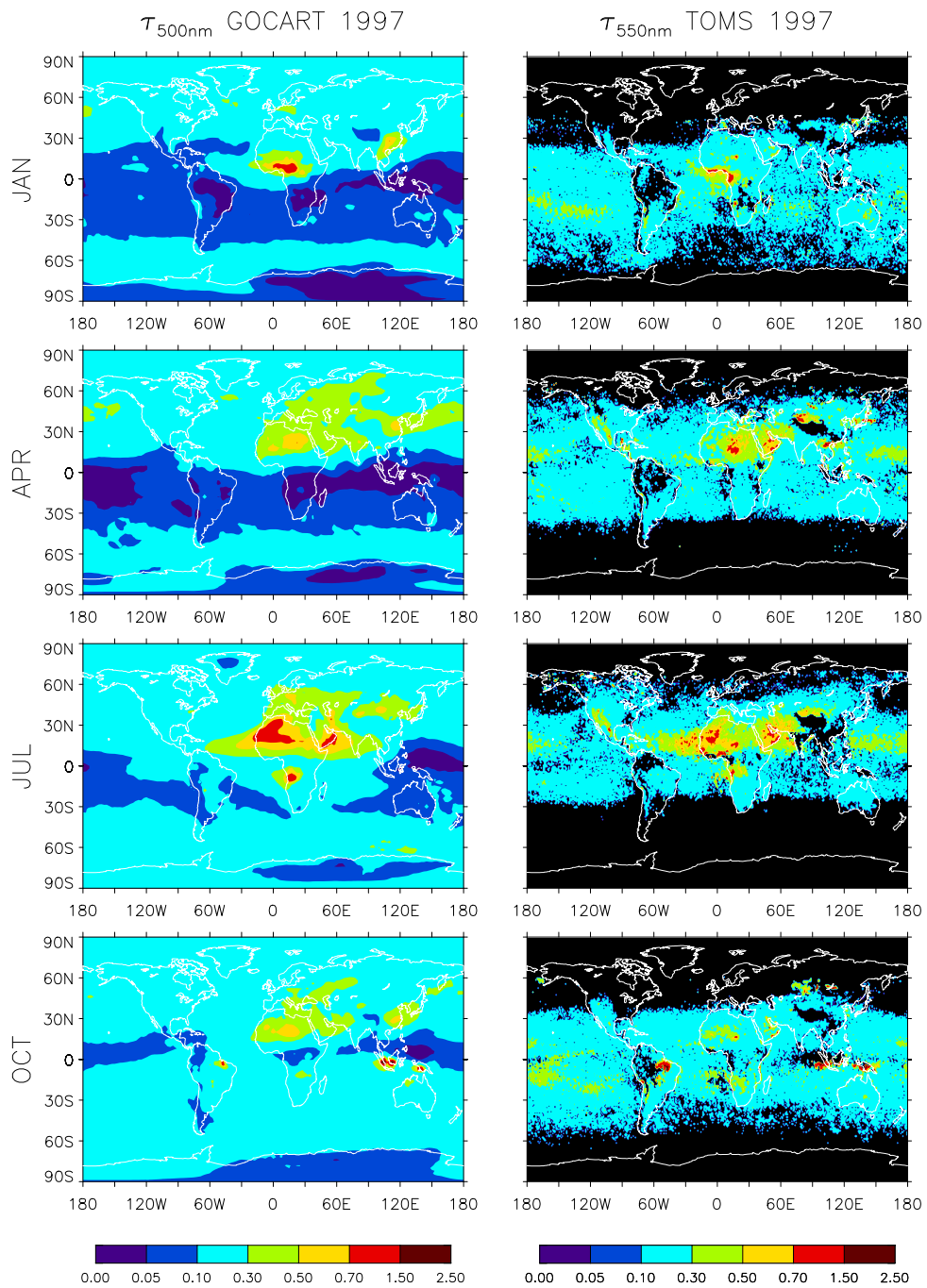


Figure 3. Aerosol optical thickness in 1997 from the GOCART model (left column) and the TOMS retrieval (right column). TOMS data are from Torres et al., 2001.

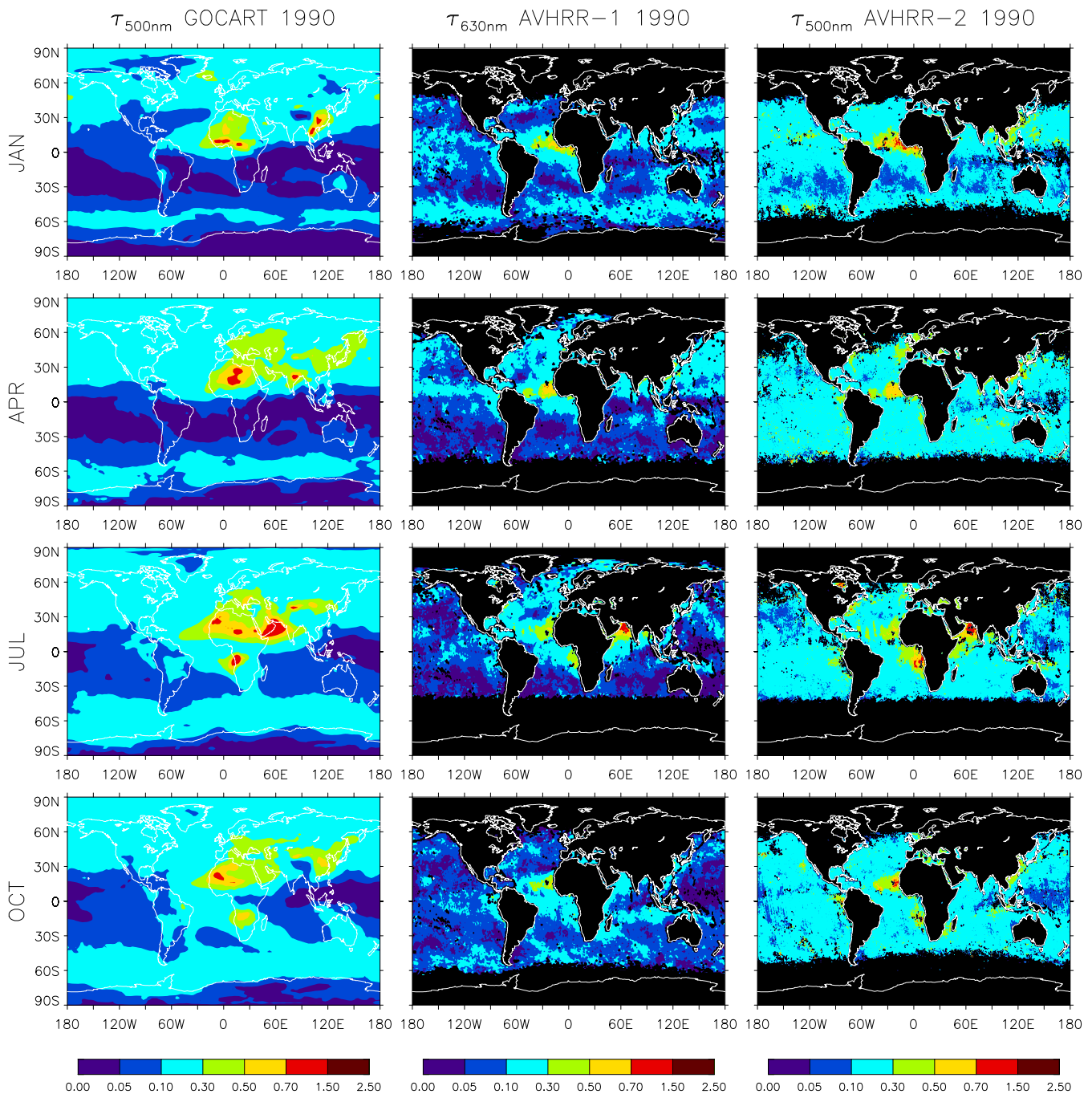


Figure 4. Aerosol optical thickness in 1990 from the GOCART model (left column) and the 1-channel (AVHRR-1) and 2-channel (AVHRR-2) retrievals.

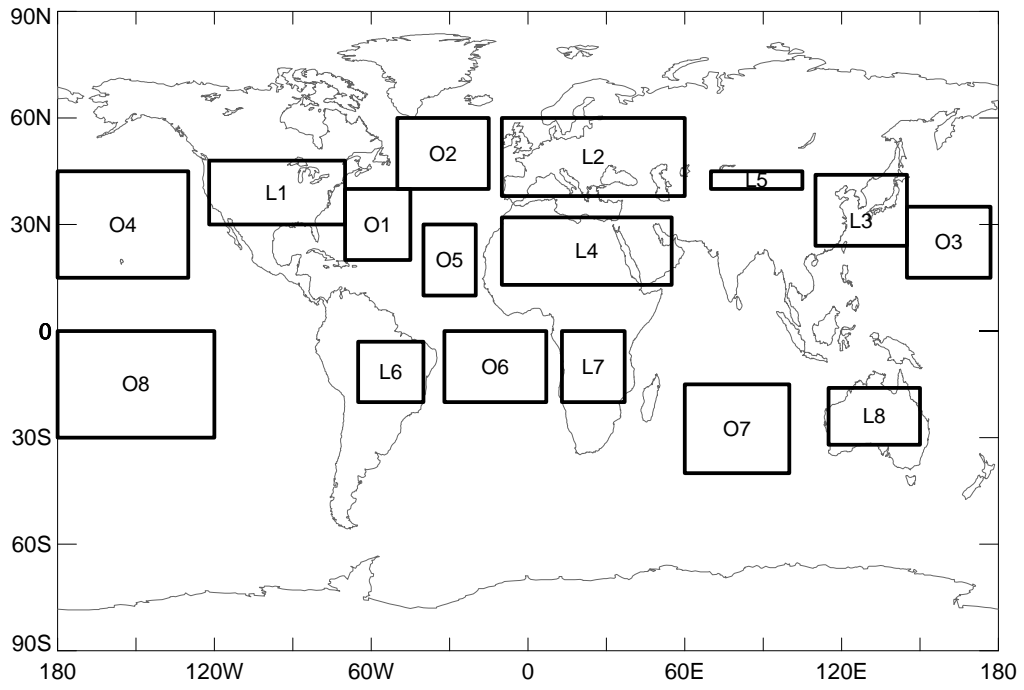


Figure 5

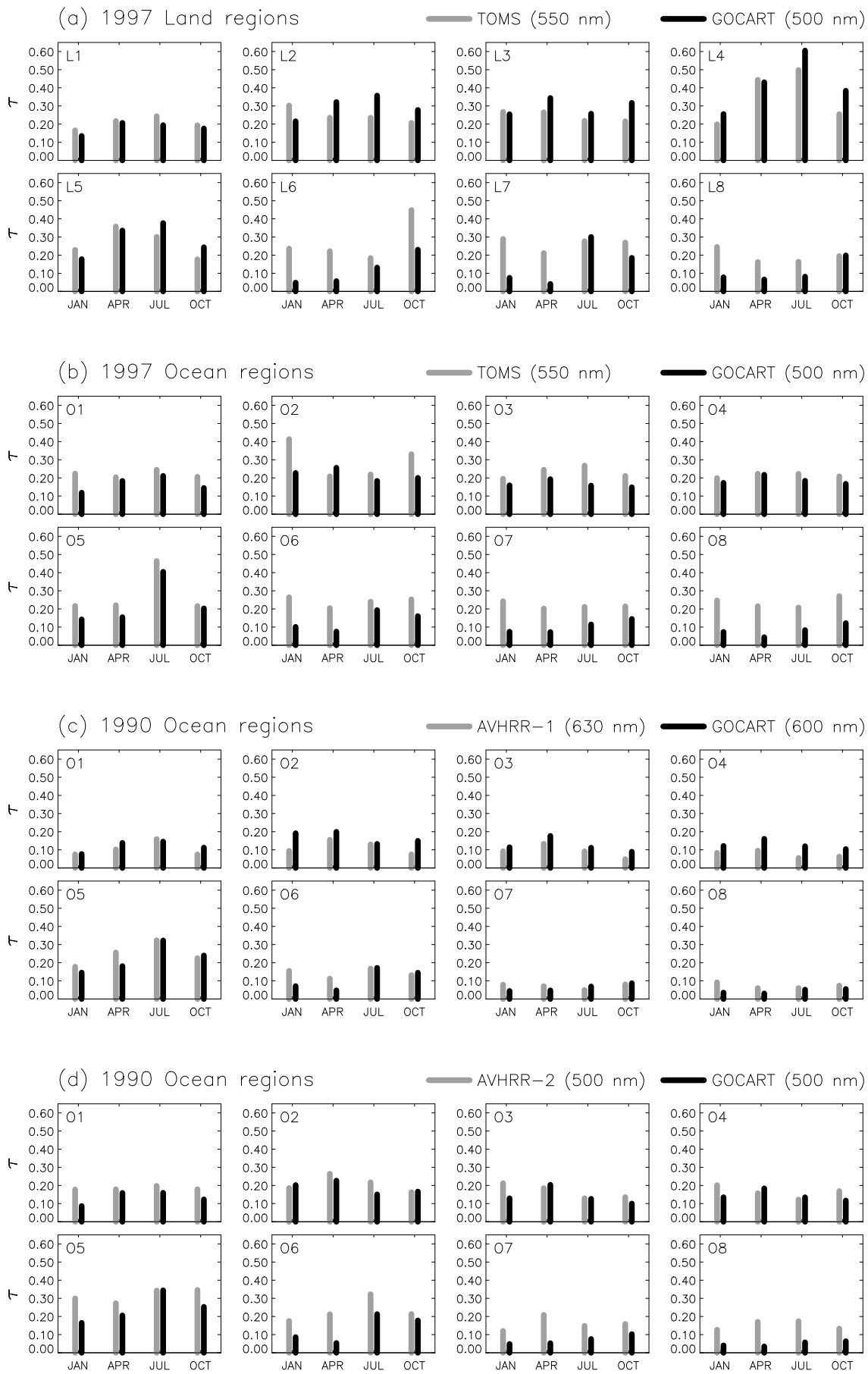


Figure 6

GOCART alpha at 600-800 nm

AVHRR-2 alpha at 630-840 nm

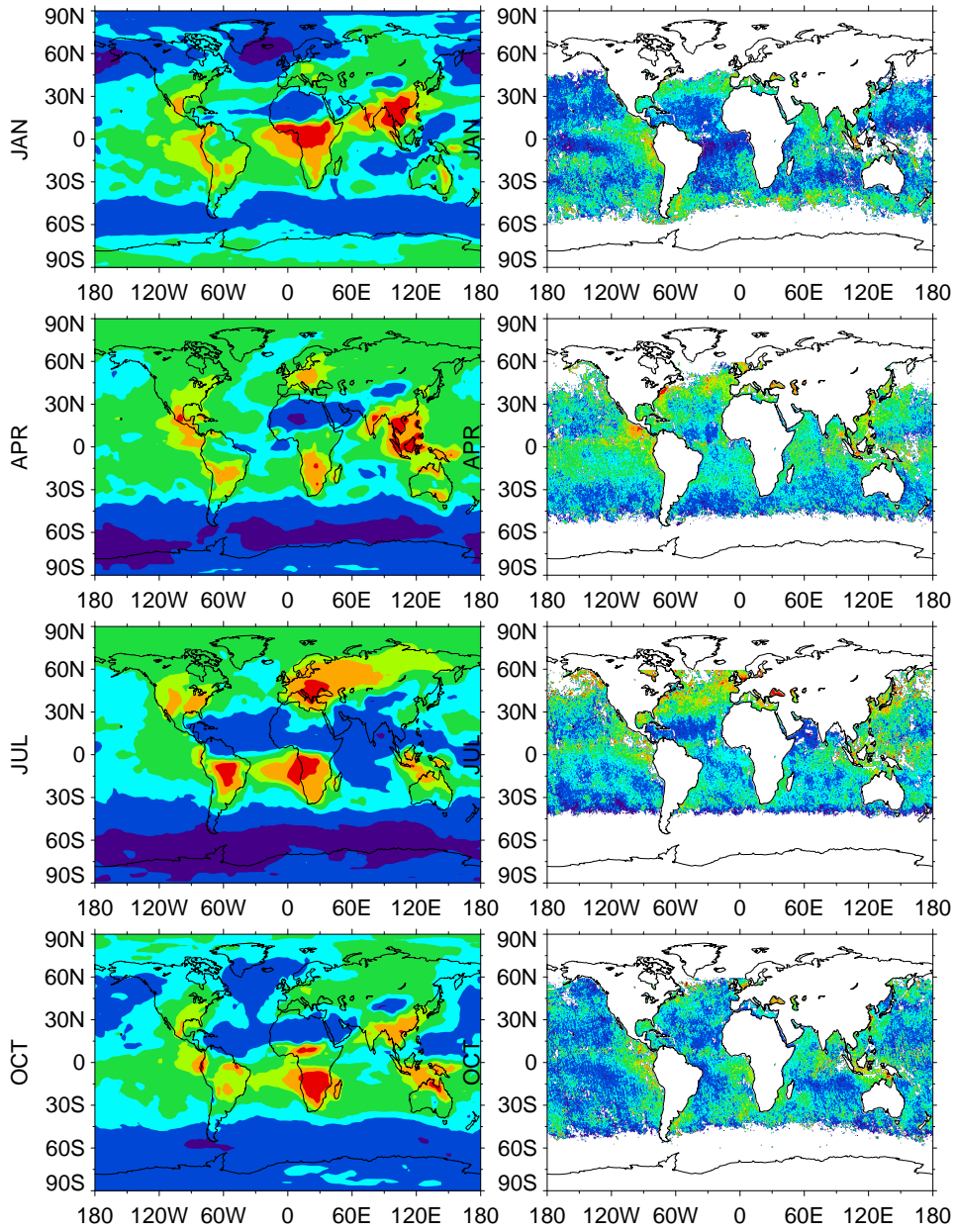


Figure 7. Angstrom exponent from the GOCART model and from AVHRR-2 retrieval for 1990.



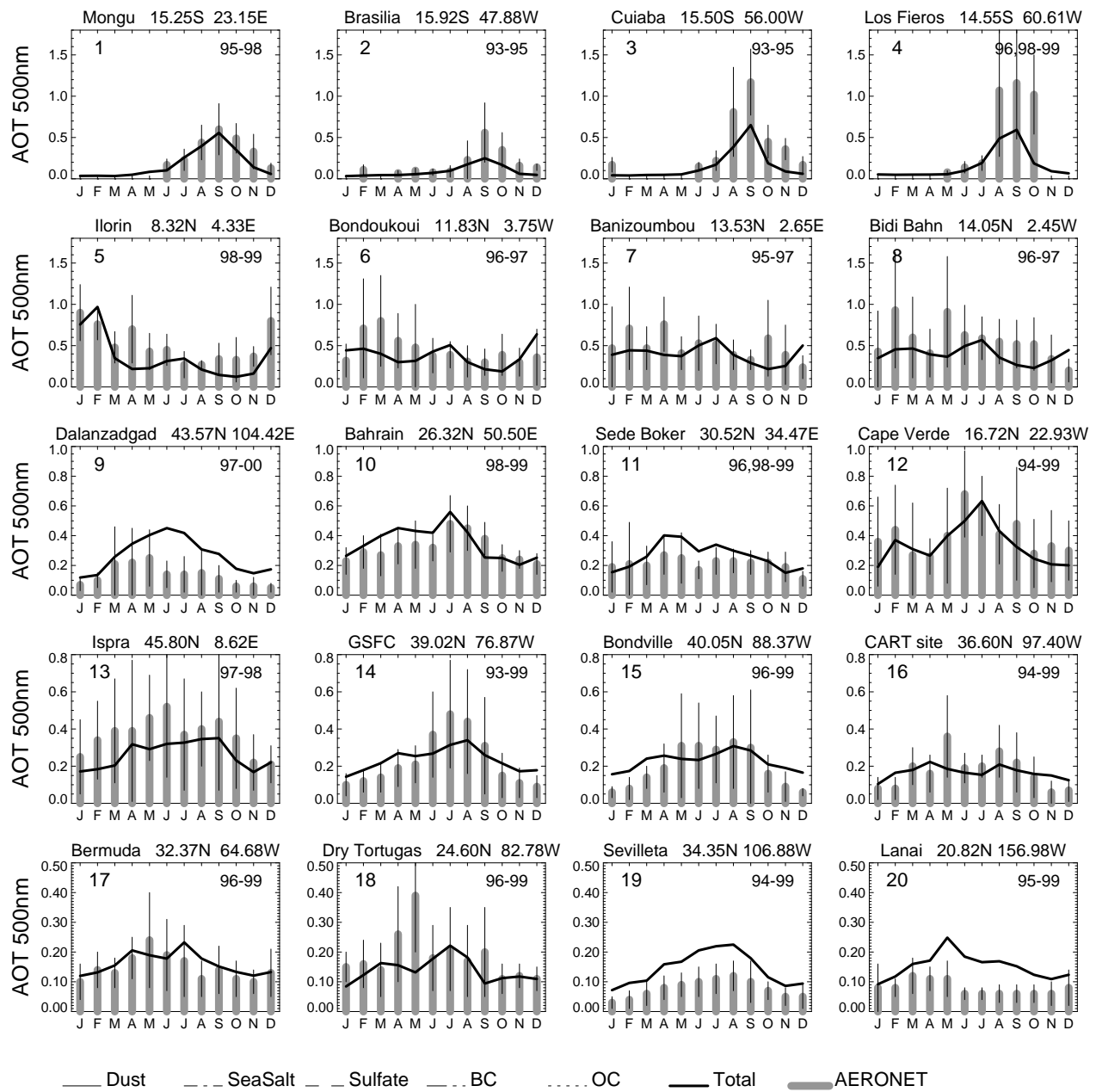


Figure 8. Aerosol optical thickness at 500 nm.

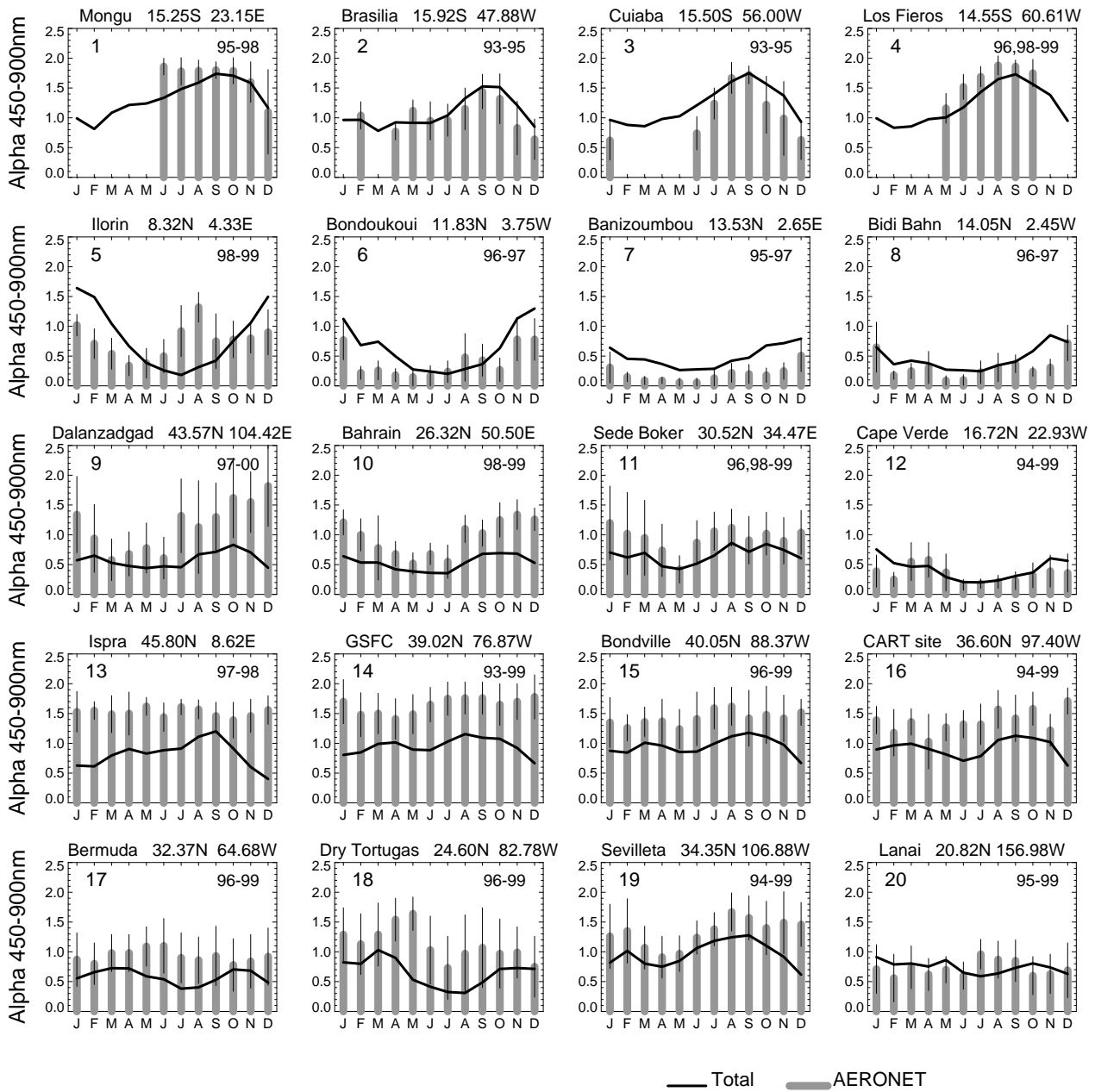


Figure 9. Angstrom exponent.

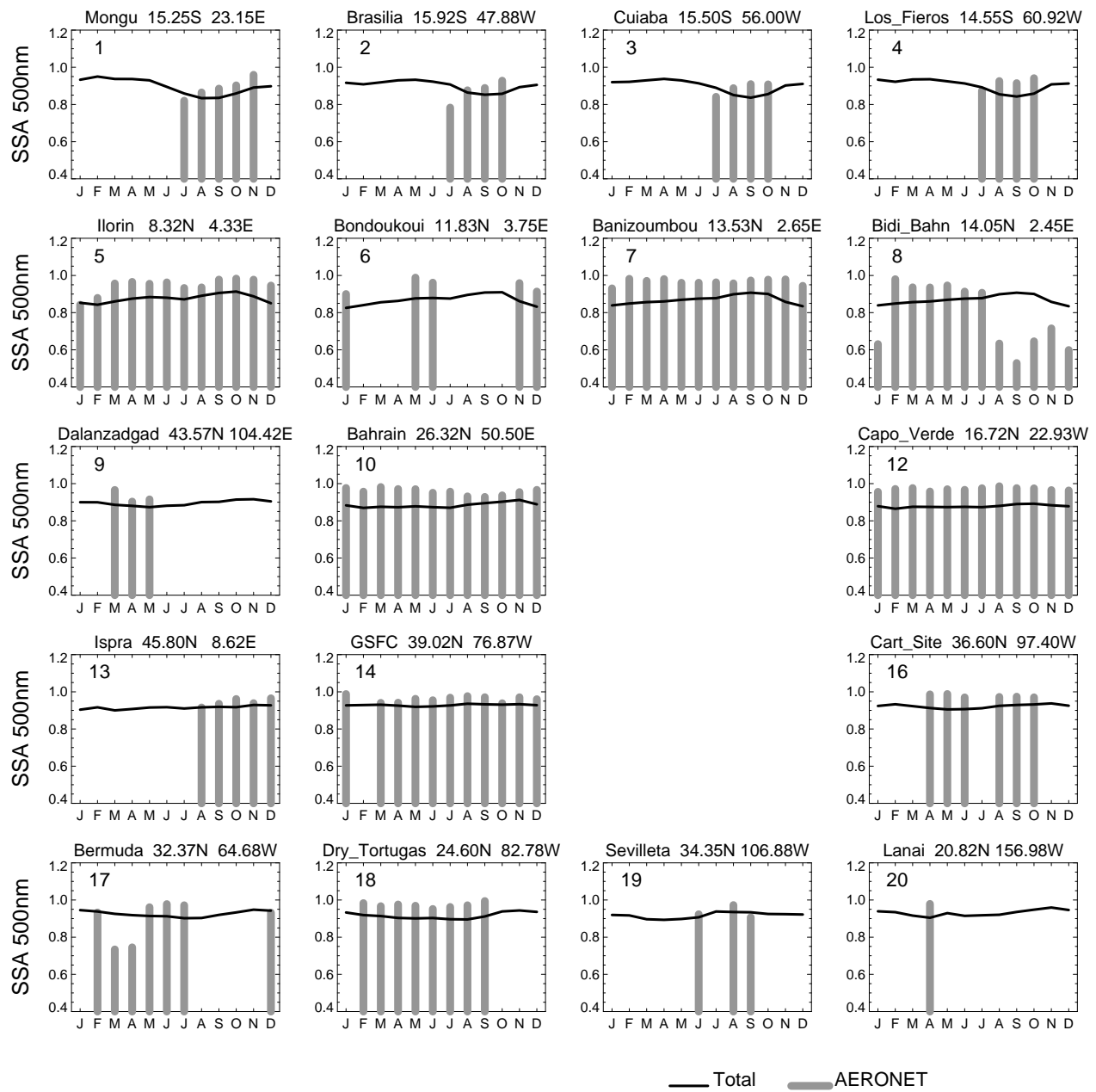


Figure 10. Single scattering albedo at 500 nm.